Supporting Information

Design criteria for high-temperature Single Molecule Magnets

Nicholas F. Chilton

School of Chemistry, The University of Manchester, Oxford Road, Manchester, M19 3PL, United Kingdom
nicholas.chilton@manchester.ac.uk

Contents

Geometry optimization

Model ligand geometries were optimized with Density Functional Theory (DFT) as described below using the B3LYP functional[1–3] with DFTD3 dispersion corrections[4,5] and the def2-TZVP basis[6,7] as implemented in ORCA 3.0.2.[8]

L_1 = $^-N(SiH_3)_2$

The Si-N-Si angle and N-Si bond lengths for L_1 were taken from average crystallographic values for similar species (Si-N-Si = 135(5)° and N-Si = 1.71(4) Å)[9–11] and the hydrogen positions were optimized.

L_2 = $^-C(SiH_3)_3$

The Si-C-Si angles and C-Si bond lengths for L_2 were taken from average crystallographic values for similar species (Si-C-Si = 115(1)° and C-Si = 1.84(1) Å)[12,13] and the hydrogen positions were optimized.

L_3 = $^-CH(SiH_3)_2$

The Si-C-Si angle and C-Si bond lengths for L_3 were taken from average crystallographic values for similar species (Si-C-Si = 122(3)° and C-Si = 1.82(2) Å),[14–17] the methyl proton fixed with Si-C-H = 90° and C-H = 1.0 Å and the remaining hydrogen positions were optimized.

THF

The entire molecule was optimized.

*[Sm{C(SiMe$_3$)$_3$}$_2$] (**2**)*

Hydrogen atoms were added and their positions optimized with Ca^{2+} as a diamagnetic substituent for Sm^{2+}.

Ab initio calculations

Ab initio calculations were performed using the CASSCF/RASSI/SINGLE_ANISO approach,[18–20] using MOLCAS 7.8.[21–23] For all calculations the Dy atom was treated with the ANO-RCC-VTZP basis, the N or C donors and the Si atoms with the ANO-RCC-VDZP basis, while all other atoms were treated with treated with the ANO-RCC-VDZ basis.[24–27] The two electron integrals were Cholesky decomposed with the default thresholds. The $4f^9$ configuration of Dy^{III} was modelled with a complete active space of 9 electrons in 7 orbitals, where 21 sextets, 224 quartets and 158 doublets were included in the orbital optimization and 21 sextets, 128 quartets and 130 doublets were mixed by spin-orbit coupling. The *ab initio* results, parameterized by a set of crystal field parameters where the z-axis is the main magnetic axis of the ground Kramers doublet,[28] were then utilized to estimate the energy barriers to the reversal of magnetization, U_{eff}.

U_{eff} barrier construction

Firstly it is ensured that the crystal field parameters are such that the main magnetic moment of the ground Kramers doublet is taken as the quantization axis. Then the magnetic transition probability is calculated with PHI[29] as the average of the x, y and z magnetic perturbations linking two states, $P_{ab} = \frac{g_J{}^2}{3}\left(\left|\langle\psi_a|\hat{J}_x|\psi_b\rangle\right|^2 + \left|\langle\psi_a|\hat{J}_y|\psi_b\rangle\right|^2 + \left|\langle\psi_a|\hat{J}_z|\psi_b\rangle\right|^2\right)$, where $|\psi_a\rangle$ and $|\psi_b\rangle$ are two eigenvectors of the crystal field Hamiltonian. This matrix is symmetric with zeroes on the diagonal. The system is initialized in the ground state with negative magnetization along the quantization axis and any transition elements involving a decrease in magnetic moment are set to zero. The probability of departure from each state is normalized to unity and all possible pathways leading to the positively magnetized component of the ground doublet are examined (keeping in mind that steps which decrease the magnetization are disallowed). The probability for each pathway is taken as the product of the probabilities for each step, normalized such that the sum of the probabilities for all pathways is unity. The energy barrier for each pathway is assigned as the maximum energy encountered in that pathway and the overall U_{eff} is then the sum of all possible relaxation pathways weighted by their probabilities. It must be stressed that the method used here to estimate the U_{eff} value for each calculation is not strictly correct as this of course neglects the phonon density of states of these hypothetical compounds as well as the alteration of the crystal field during vibrational modes. However the model is useful in comparison to examine the trends upon complex deformation. Furthermore it is noted that the use of truncated model ligands leads to a small alteration of the calculated U_{eff} values: U_{eff} calculated for **1Dy** with this approach yields U_{eff} = 1837 cm^{-1}, while for a comparable complex of L_1 U_{eff} = 2060 cm^{-1} (θ = 175° and φ = 40°). Likewise for **2Dy** and **3Dy**, the barriers are calculated to be U_{eff} = 1247 cm^{-1} and U_{eff} = 1484 cm^{-1}, respectively, while for comparable complexes of L_2 U_{eff} = 1573 cm^{-1} (θ = 135° and φ = 50°) and U_{eff} = 1847 cm^{-1} (θ = 145° and φ = 60°), respectively.

Table S1. *Ab initio* calculated electronic states for **2Dy**.

E (cm^{-1})	g_x	g_y	g_z	g_z **angle (°)**
0	0.0000	0.0000	19.8736	-
352	0.0013	0.0015	16.9747	0.4
657	0.0332	0.0379	14.0905	0.3
907	0.3792	0.3923	11.2272	0.4
1094	2.5017	2.2152	8.1411	1.1
1219	8.4877	5.4345	4.2645	0.5
1318	15.2567	2.2021	1.1156	0.3
1408	19.5269	0.1921	0.0932	0.4

Table S2. Crystal-field calculated electronic states for **2Dy**, using the *ab initio* crystal field parameters.

E (cm^{-1})	g_x	g_y	g_z	g_z angle (°)	*Wavefunctions*
0	0.0000	0.0000	19.9774	-	$100\%\|\pm 15/2\rangle$
350	0.0013	0.0016	17.2191	0.4	$98\%\|\pm 13/2\rangle + 2\%\|\pm 9/2\rangle$
657	0.0334	0.0386	14.3976	0.3	$94\%\|\pm 11/2\rangle + 5\%\|\pm 7/2\rangle$
908	0.3748	0.3916	11.5364	0.5	$88\%\|\pm 9/2\rangle + 10\%\|\pm 5/2\rangle$ $+2\%\|\pm 13/2\rangle$
1094	2.2575	2.5310	8.3776	1.2	$76\%\|\pm 7/2\rangle + 17\%\|\pm 3/2\rangle$ $+5\%\|\pm 11/2\rangle + 2\%\|\mp 1/2\rangle$
1218	8.5837	5.5547	4.3417	0.4	$34\%\|\pm 5/2\rangle + 21\%\|\mp 5/2\rangle$ $+17\%\|\pm 1/2\rangle + 12\%\|\mp 1/2\rangle$ $+5\%\|\pm 9/2\rangle + 3\%\|\mp 9/2\rangle + 3\%\|\mp 7/2\rangle$ $+2\%\|\pm 7/2\rangle + 2\%\|\pm 3/2\rangle + 2\%\|\mp 3/2\rangle$
1316	15.3925	2.1481	1.0951	0.3	$47\%\|\pm 3/2\rangle + 23\%\|\mp 5/2\rangle$ $+13\%\|\mp 1/2\rangle + 11\%\|\pm 7/2\rangle$ $+3\%\|\mp 3/2\rangle + 2\%\|\mp 9/2\rangle$ $+1\%\|\pm 1/2\rangle + 2\%\|\pm 5/2\rangle$
1408	19.6698	0.1701	0.0840	0.4	$53\%\|\pm 1/2\rangle + 28\%\|\mp 3/2\rangle$ $+10\%\|\pm 5/2\rangle + 3\%\|\mp 7/2\rangle$ $+3\%\|\mp 1/2\rangle + 2\%\|\pm 3/2\rangle + 1\%\|\mp 5/2\rangle$

Table S3. *Ab initio* calculated crystal field parameters for **2Dy**.

Parameter	Value (cm^{-1})
B_2^{-2}	2.01962721927927E-01
B_2^{-1}	9.90535471369045E-02
B_2^0	-7.97415315824689E+00
B_2^1	9.45043914084932E-02
B_2^2	3.09623722913212E+00
B_4^{-4}	2.55865420502294E-03
B_4^{-3}	2.94433661425981E-04
B_4^{-2}	2.32410301921615E-03
B_4^{-1}	-5.60993397492546E-04
B_4^0	-2.34093970354183E-03
B_4^1	1.04610326782185E-03
B_4^2	1.35613368433382E-02
B_4^3	1.24933000434739E-02
B_4^4	-1.52335628295406E-03
B_6^{-6}	-2.58151378671642E-05
B_6^{-5}	-3.74582627683468E-05
B_6^{-4}	-3.78467505427757E-05
B_6^{-3}	-1.09824415321907E-05
B_6^{-2}	-2.61195638356284E-07
B_6^{-1}	-3.81531217138823E-06
B_6^0	1.06249156432690E-05
B_6^1	-2.25869579446961E-05
B_6^2	-1.25083861866480E-04
B_6^3	2.43263765905571E-06
B_6^4	1.46628048009982E-05
B_6^5	-5.73140016168279E-05
B_6^6	-7.58183352474061E-07

Table S4. *Ab initio* calculated electronic states for **3Dy**.

E (cm^{-1})	g_x	g_y	g_z	g_z angle (°)
0	0.0000	0.0000	19.8900	-
413	0.0007	0.0008	17.0056	0.7
782	0.0167	0.0181	14.1508	0.3
1079	0.2129	0.2202	11.3113	1.3
1290	1.8349	1.8075	8.2396	4.0
1418	7.7901	6.3410	4.1462	1.9
1518	15.1435	2.1177	0.8969	0.4
1645	19.5646	0.0545	0.0278	0.5

Table S5. Crystal-field calculated electronic states for **3Dy**, using the *ab initio* crystal field parameters.

E (cm^{-1})	g_x	g_y	g_z	g_z angle (°)	*Wavefunctions*
0	0.0000	0.0000	19.9888	-	$100\%\|\pm 15/2\rangle$
410	0.0007	0.0008	17.2774	0.8	$99\%\|\pm 13/2\rangle + 1\%\|\pm 9/2\rangle$
784	0.0155	0.0171	14.5132	0.3	$97\%\|\pm 11/2\rangle + 3\%\|\pm 7/2\rangle$
1080	0.2095	0.2202	11.6693	1.3	$92\%\|\pm 9/2\rangle + 7\%\|\pm 5/2\rangle$ $+1\%\|\pm 13/2\rangle$
1289	1.8246	1.8611	8.5109	3.8	$80\%\|\pm 7/2\rangle + 15\%\|\pm 3/2\rangle$ $+3\%\|\pm 11/2\rangle + 1\%\|\mp 1/2\rangle$
1415	7.8311	6.3969	4.2759	1.6	$56\%\|\pm 5/2\rangle + 30\%\|\pm 1/2\rangle$ $+5\%\|\pm 9/2\rangle + 4\%\|\mp 3/2\rangle + 4\%\|\mp 7/2\rangle$
1516	15.2198	2.1256	0.9183	0.4	$40\%\|\pm 3/2\rangle + 20\%\|\mp 5/2\rangle$ $+10\%\|\mp 1/2\rangle + 10\%\|\mp 3/2\rangle$ $+8\%\|\pm 7/2\rangle + 4\%\|\pm 5/2\rangle + 4\%\|\pm 1/2\rangle$ $+2\%\|\mp 7/2\rangle + 1\%\|\mp 9/2\rangle$
1645	19.6974	0.0544	0.0279	0.3	$51\%\|\pm 1/2\rangle + 28\%\|\mp 3/2\rangle$ $+11\%\|\pm 5/2\rangle + 3\%\|\pm 3/2\rangle$ $+3\%\|\mp 7/2\rangle + 3\%\|\mp 1/2\rangle + 1\%\|\mp 5/2\rangle$

Table S6. *Ab initio* calculated crystal field parameters for **3Dy**.

Parameter	Value (cm^{-1})
B_2^{-2}	-1.54497001881025E-02
B_2^{-1}	1.60949328578478E-02
B_2^0	-9.33457494690100E+00
B_2^1	1.92878051778270E-01
B_2^2	3.09394290563682E+00
B_4^{-4}	3.07220302128604E-04
B_4^{-3}	3.81913879110261E-04
B_4^{-2}	-4.06823584071651E-04
B_4^{-1}	5.97986290483851E-04
B_4^0	-3.17331013820649E-03
B_4^1	2.03510214939157E-03
B_4^2	7.92115989320873E-03
B_4^3	1.51186002032762E-02
B_4^4	6.69929061801084E-04
B_6^{-6}	3.85332707821224E-06
B_6^{-5}	1.19499993568456E-05
B_6^{-4}	-6.17502794576279E-06
B_6^{-3}	-1.54198236037387E-05
B_6^{-2}	1.78740571440496E-06
B_6^{-1}	-1.45391436271930E-05
B_6^0	1.81386270585825E-05
B_6^1	-5.27156054171306E-05
B_6^2	-8.73350847517333E-05
B_6^3	-7.77107936900869E-06
B_6^4	-2.69589025010664E-05
B_6^5	-5.02559403686099E-05
B_6^6	2.60302918806461E-05

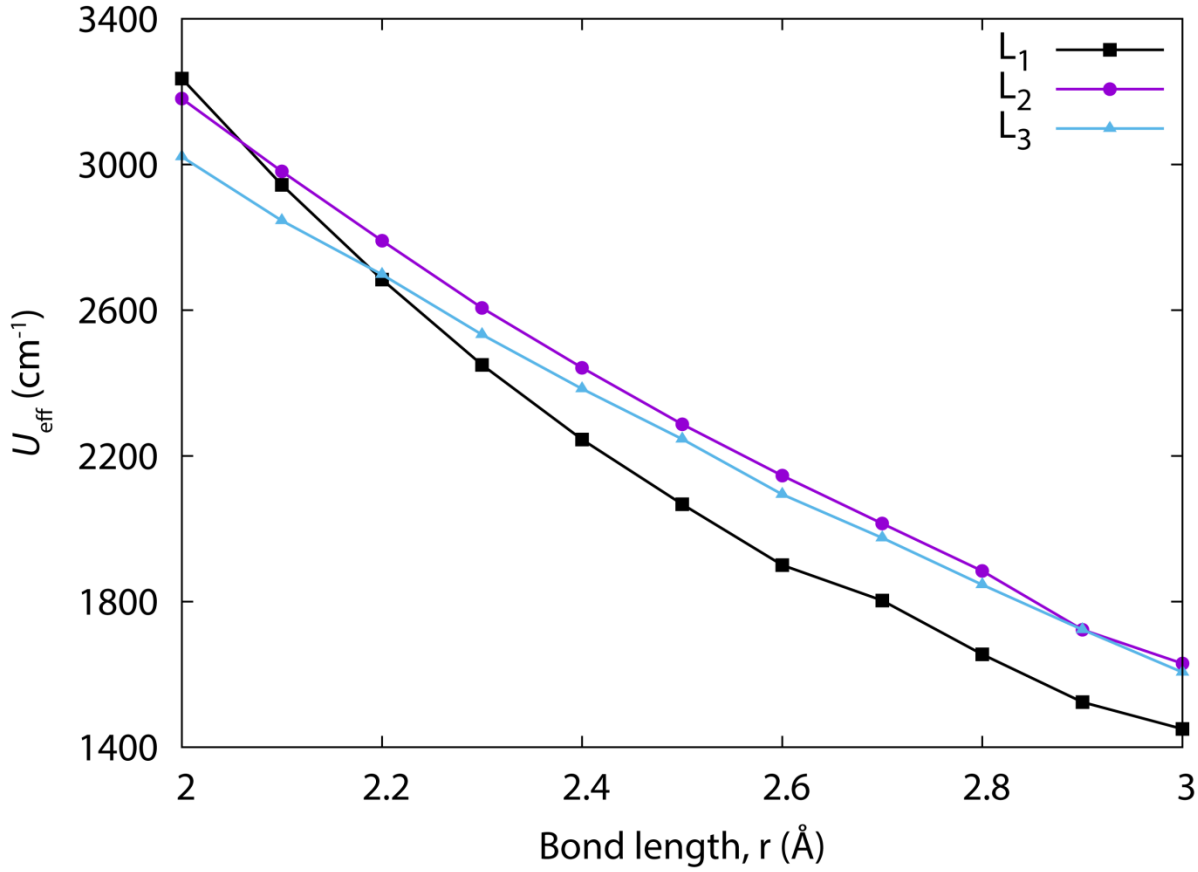

Figure S1. Calculated barrier to magnetization reversal U_{eff} as a function of the Dy-E bond length r, for θ = 180° and φ = 90°.

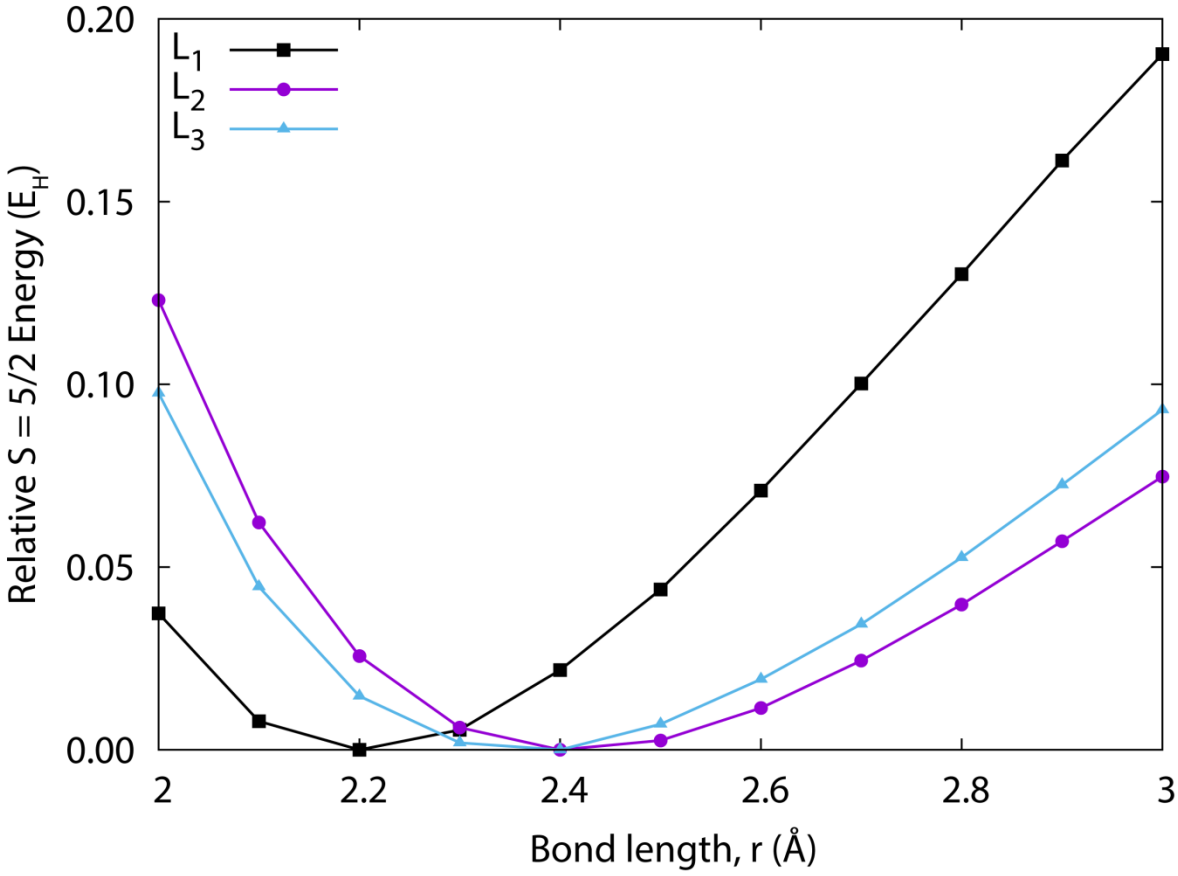

Figure S2. Relative energy of the *S* = 5/2 CASSCF wavefunction as a function of the Dy-E bond length r, for θ = 180° and φ = 90°.

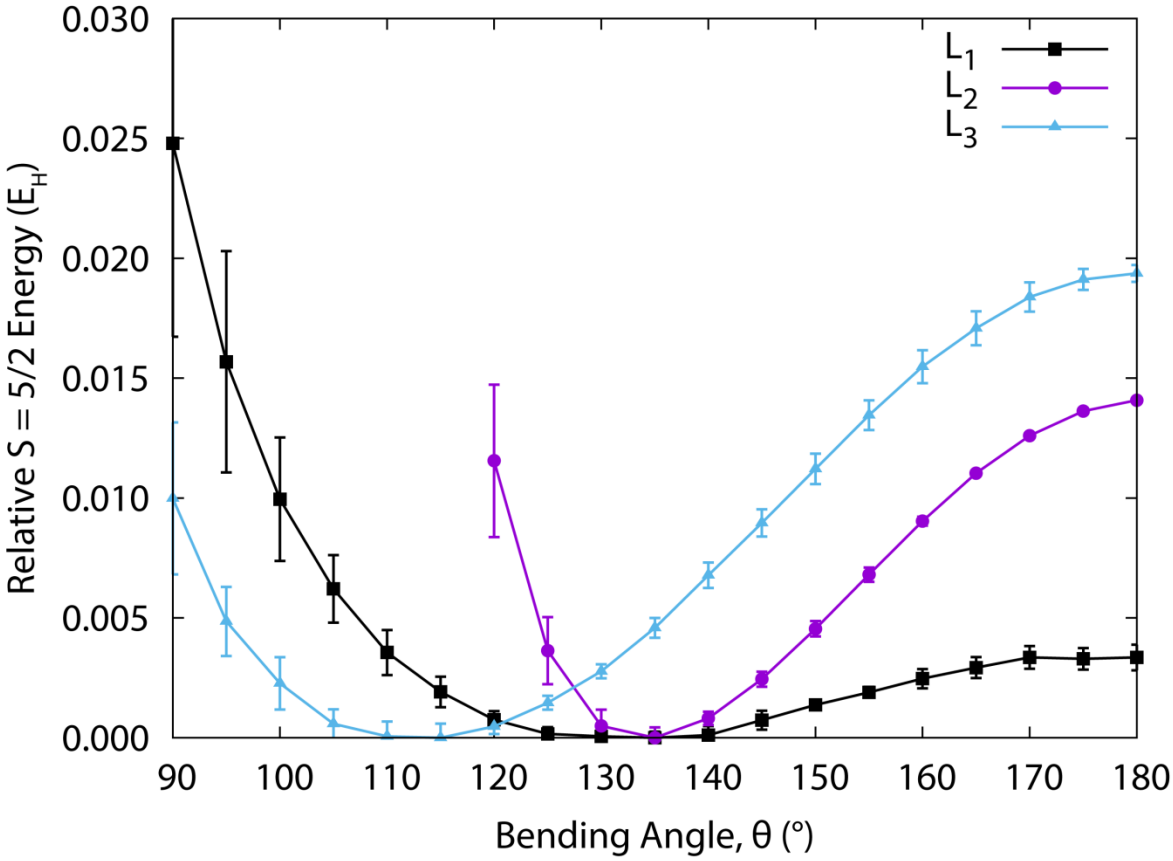

Figure S3. Relative energy of the *S* = 5/2 CASSCF wavefunction as a function of the E-Dy-E bending angle θ, averaged for all torsion angles φ. Error bars are one standard deviation from the mean of the torsion angles φ.

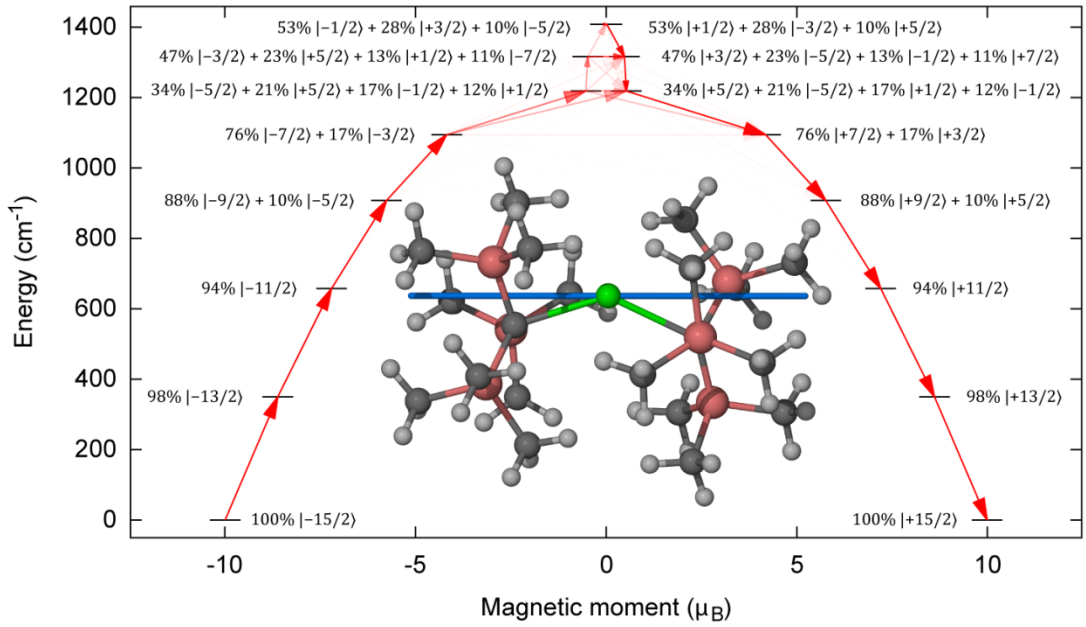

Figure S4. Zero-field magnetic transition probabilities within the ground multiplet for **2Dy**. The x-axis shows the magnetic moment of each state along the main magnetic axis of the molecule. Relaxation commences from the $|-15/2\rangle$ state and only includes pathways which reverse the magnetization. The transparency of each arrow is proportional to the normalized transition probability. Inset: main magnetic axis of the ground Kramers doublet for **2Dy** (blue rod), Dy = green, Si = pink, C = grey and H = white.

References

(1) Lee, C.; Yang, W.; Parr, R. G. *Phys. Rev. B* **1988**, *37*, 785-789.
(2) Becke, A. D. *Phys. Rev. A* **1988**, *38*, 3098-3100.
(3) Becke, A. D. *J. Chem. Phys.* **1993**, *98*, 5648-5652.
(4) Grimme, S.; Antony, J.; Ehrlich, S.; Krieg, H. *J. Chem. Phys.* **2010**, *132*, 154104.
(5) Grimme, S.; Ehrlich, S.; Goerigk, L. *J. Comput. Chem.* **2011**, *32*, 1456-1465.
(6) Schäfer, A.; Horn, H.; Ahlrichs, R. *J. Chem. Phys.* **1992**, *97*, 2571-2577.
(7) Weigend, F.; Ahlrichs, R. *Phys. Chem. Chem. Phys.* **2005**, *7*, 3297-3305.
(8) Neese, F. *Wiley Interdiscip. Rev. Comput. Mol. Sci.* **2012**, *2*, 73-78.
(9) Chilton, N. F.; Goodwin, C. A. P.; Mills, D. P.; Winpenny, R. E. P. *Chem. Commun.* **2015**, *51*, 101-103.
(10) Goodwin, C. A. P.; Tuna, F.; McInnes, E. J. L.; Liddle, S. T.; McMaster, J.; Vitorica-Yrezabal, I. J.; Mills, D. P. *Chem. – Eur. J.* **2014**, *20*, 14579-14583.
(11) Goodwin, C. A. P.; Joslin, K. C.; Lockyer, S. J.; Formanuik, A.; Morris, G. A.; Ortu, F.; Vitorica-Yrezabal, I. J.; Mills, D. P. *Organometallics* **2015**, doi: 10.1021/om501123e
(12) Eaborn, C.; Hitchcock, P. B.; Izod, K.; Smith, J. D. *J. Am. Chem. Soc.* **1994**, *116*, 12071-12072.
(13) Qi, G.; Nitto, Y.; Saiki, A.; Tomohiro, T.; Nakayama, Y.; Yasuda, H. *Tetrahedron* **2003**, *59*, 10409-10418.
(14) Avent, A. G.; Caro, C. F.; Hitchcock, P. B.; Lappert, M. F.; Li, Z.; Wei, X.-H. *Dalton Trans.* **2004**, 1567-1577.
(15) Hitchcock, P. B.; Khvostov, A. V.; Lappert, M. F. *J. Organomet. Chem.* **2002**, *663*, 263.
(16) Barker, G. K.; Lappert, M. F. *J. Organomet. Chem.* **1974**, *76*, C45.
(17) Hitchcock, P. B.; Lappert, M. F.; Smith, R. G.; Bartlett, R. A.; Power, P. P. *J. Chem. Soc. Chem. Commun.* **1988**, 1007-1009.
(18) Ungur, L.; Chibotaru, L. F. *Phys. Chem. Chem. Phys.* **2011**, *13*, 20086-20090.
(19) Blagg, R. J.; Ungur, L.; Tuna, F.; Speak, J.; Comar, P.; Collison, D.; Wernsdorfer, W.; McInnes, E. J. L.; Chibotaru, L. F.; Winpenny, R. E. P. *Nat. Chem.* **2013**, *5*, 673-678.
(20) Ungur, L.; Le Roy, J. J.; Korobkov, I.; Murugesu, M.; Chibotaru, L. F. *Angew. Chem. Int. Ed.* **2014**, *53*, 4413-4417.
(21) Karlström, G.; Lindh, R.; Malmqvist, P.-Å.; Roos, B. O.; Ryde, U.; Veryazov, V.; Widmark, P.-O.; Cossi, M.; Schimmelpfennig, B.; Neogrady, P.; Seijo, L. *Comput. Mater. Sci.* **2003**, *28*, 222-239.
(22) Veryazov, V.; Widmark, P.; Serrano-Andrés, L.; Lindh, R.; Roos, B. O. *Int. J. Quantum Chem.* **2004**, *100*, 626-635.
(23) Aquilante, F.; De Vico, L.; Ferré, N.; Ghigo, G.; Malmqvist, P.; Neogrády, P.; Pedersen, T. B.; Pitoňák, M.; Reiher, M.; Roos, B. O.; Serrano-Andrés, L.; Urban, M.; Veryazov, V.; Lindh, R. *J. Comput. Chem.* **2010**, *31*, 224-247.
(24) Roos, B. O.; Veryazov, V.; Widmark, P.-O. *Theor. Chem. Acc.* **2004**, *111*, 345-351.
(25) Roos, B. O.; Lindh, R.; Malmqvist, P.-Å.; Veryazov, V.; Widmark, P.-O. *J. Phys. Chem. A* **2004**, *108*, 2851-2858.
(26) Roos, B. O.; Lindh, R.; Malmqvist, P.-Å.; Veryazov, V.; Widmark, P.-O. *J. Phys. Chem. A* **2005**, *109*, 6575-6579.
(27) Roos, B. O.; Lindh, R.; Malmqvist, P.-Å.; Veryazov, V.; Widmark, P.-O. *Chem. Phys. Lett.* **2005**, *409*, 295-299.
(28) Chibotaru, L. F.; Ungur, L. *J. Chem. Phys.* **2012**, *137*, 064112.
(29) Chilton, N. F.; Anderson, R. P.; Turner, L. D.; Soncini, A.; Murray, K. S. *J. Comput. Chem.* **2013**, *34*, 1164-1175.